Proceedings Paper:
Sen, B. and Wang, J. orcid.org/0000-0003-4870-3744 (2014) Stator inter-turn fault detection in SPM machines using PWM ripple current measurement. In: Proceedings of 7th IET International Conference on Power Electronics, Machines and Drives (PEMD 2014). 7th IET International Conference on Power Electronics, Machines and Drives (PEMD 2014), 08-10 Apr 2014, Manchester, UK. Institution of Engineering and Technology (IET)

https://doi.org/10.1049/cp.2014.0288

Stator Inter-turn Fault Detection in SPM Machines Using PWM Ripple Current Measurement

B. Sen*, J. Wang*

* *The University of Sheffield, Sheffield, United Kingdom, elp11bs@sheffield.ac.uk , j.b.wang@sheffield.ac.uk*

Keywords: Fault diagnosis, PWM harmonics, permanent magnet drives, high frequency fault detection.

Abstract

In this paper a novel method of inter-turn fault detection based on measurement of high frequency pulse width modulation (PWM) ripple current is proposed. The method uses the ripple current generated by the inverter itself as a means to detect inter-turn fault. High frequency impedance behaviours of healthy and faulted windings are analysed and modelled, and ripple current signature due to inter-turn faults is quantified. A simple analogue circuit is designed to extract the PWM ripple current via an RMS band-pass filter and the filtered RMS current is used for fault detection. In addition, the method also identifies the faulted phase. The method is tested in simulation on a five phase alternate slot wound SPM machine.

1 Introduction

Permanent magnet(PM) motors are increasingly being favoured as the motor of choice for electric vehicle application due to their high power density and overall high efficiency [1]. For providing high availability in electric vehicles reliable diagnostics of motor operational states and health is essential. Internal combustion engines based vehicles already have diagnostics features like the “check engine” light which provides the user with a warning of a problem with the engine and possible early warning signal to an impending engine failure. A similar functionality would be highly desirable in electric vehicles.

Industrial surveys have shown that a large percentage of motor failures (21-36%) result from a fault related to the stator winding [2]–[4]. It has been reported in [5] that most winding short circuit faults start as inter-turn faults and quickly develop into complete winding failure. In SPM machines due to presence of magnets in the rotor any electrical faults in the stator will result in high currents in the faulted turns. The high fault current will generate a local hotspot and may cause a run-away degradation of the insulation, leading to a complete winding failure. Moreover the fault current cannot be reduced simply by shut-down the traction inverter because the rotor magnets still provide the flux, unlike in case of induction machines where the fault current can be reduced by turning off the inverter. Therefore having a fault monitoring of the SPM motor enables quick application of mitigating controls to prevent a complete failure of the windings. Such a functionality commonly known as limp-home mode is essential to providing a high degree of availability, and reliability demanded in safety critical application like electric vehicles.

The stator inter-turn fault detection has been subject to intense investigation and numerous literatures exist. Detection schemes are broadly divided into fundamental quantity based [6]–[8] detection, high frequency based [9], [10] detection and motor current signature analysis (MCSA) [11]. Most of the methods under MCSA are computationally intensive since they rely on performing fast Fourier transformation (FFT) to determine harmonic components and fault signature. High frequency signal injection methods on the other hand, inject high frequency signal in the inverter voltage command and perform synchronous demodulation of currents in software to determine stator turn fault. In [9] a high frequency signal is added in the *dq* control voltages and the high frequency currents so obtained is demodulated in *dq* frame and the negative sequence component extracted to form the fault index. In [10] the method of [9] is improved further by using lookup table based calibration of the *dq* high frequency signal to reduce effect of magnetic saliency induced by load variation from affecting the detection. However, signal injection method introduces additional noise in the current and increases acoustic emissions of the motor-drive system. In addition, most of the methods fail to identify the faulted phase which is of importance in a multi-phase machine in order to initiate fault mitigation and fault tolerant operation.

Most PM motors are fed through a pulse-width modulated (PWM) drive. The drive is a natural source of high frequency signal injection into the motor due to its switching. It is this inherent source of HF signal injection that is explored in this paper for detection of turn fault. The proposed method uses the PWM ripple current generated by the drive to determine the presence of turn fault without the need to modify or inject additional HF signal. The method is also able to identify the faulted phase which is essential to implement fault mitigation strategies.

2 Machine Modelling Under Turn Fault

The machine under consideration is a 10 slot 12-pole, 5 phase SPM machine. Fig. 1 shows the geometry of the machine. This topology also known as alternate tooth wound SPM machine, is inherently fault tolerant due to both physical and magnetic separation of the coils of the winding. Fig. 2 shows

the schematic of a single winding under the turn fault condition with N_f faulted turns out of a total N number of turns.

Fig. 1: Schematic of 10 slot, 12 pole, 5 phase SPM Machine

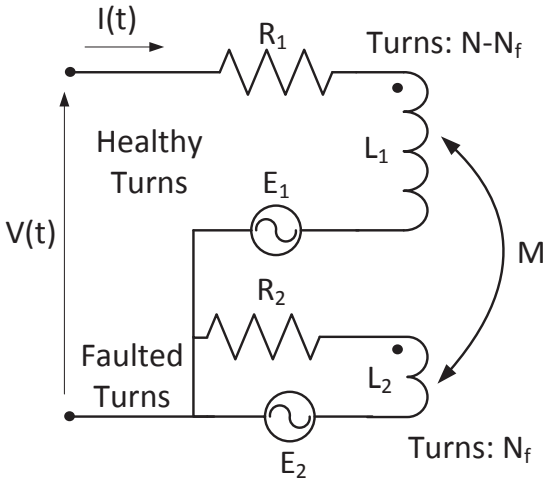

Fig. 2: Winding under fault

In order to evaluate the current ripple characteristics under PWM operation, it is useful to determine the high frequency admittance of the winding under healthy and fault conditions. For the machine under study, the admittance can be easily calculated by (1), where R_1, R_2, L_1 and L_2 are the resistance and inductance of the healthy and fault turns, respectively. M is the mutual inductance between the two winding parts.

$$Y_{eff}(j\omega) = \frac{I(j\omega)}{V(j\omega)} = \frac{1}{\left(R_1 + j\omega L_1 + \frac{\omega^2 M^2}{j\omega L_2 + R_2}\right)} \qquad (1)$$

The parameters of the machine under healthy and fault condition are given in Table 1 and Table 2 obtained by method given in [12].

Parameter	Value
Rs	0.5 Ω
Ls	2.8mH

Table I: Healthy Machine Data

	Fault Condition	
Parameter	**2 Turn fault**	**20 Turn Fault**
R_1	0.4839 Ω	0.3387 Ω
R_2	0.0161 Ω	0.1613 Ω
L_1	2.6 mH	1.3 mH
L_2	2.77 uH	0.282 mH
M	83 uH	0.5991 mH

Table II: Machine Data under Turn Fault

Fig. 3 shows the comparison of the theoretical and experimentally measured admittance of the winding using an impedance analyser. It can be observed that under the fault conditions the admittance increases particularly in the frequency range of 10-20 kHz. It is also to be noted that the admittance predicted by theory is different from that obtained from experiments especially in case of 2 turn fault. The difference between the theoretical and measured admittance is expected and attributed to external lead impedance of the fault and iron losses in the measured data which is not accounted for in the simple theoretical model. Also, as the number of faulted turns increases from healthy to 2 turn and finally to 20 turn the admittance progressively increases in the 10-20 kHz range. Higher admittance translates to lower impedance and hence higher currents for the same voltage.

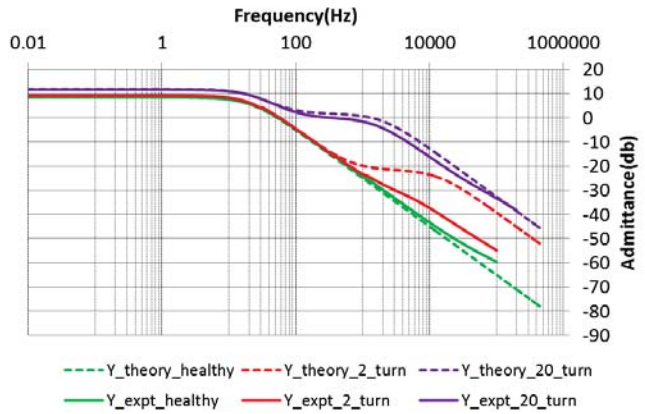

Fig. 3(a): Admittance magnitude plot of winding under fault Theoretical – dashed, Measured - dashed

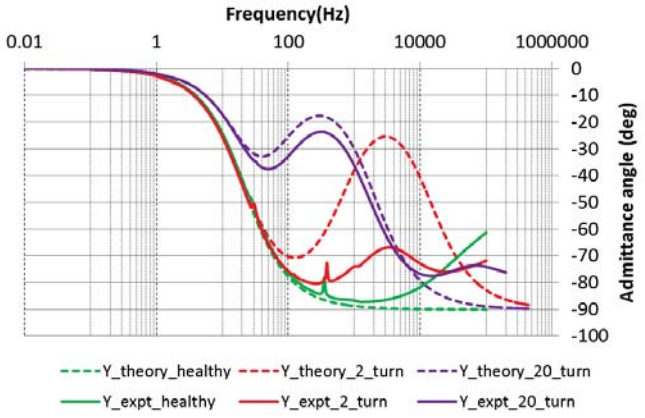

(b)

Fig. 3: Admittance angle of winding under fault Theoretical – dashed, Measured - dashed

Therefore, if the motor can be excited with a voltage in the high frequency range of 10 kHz-20 kHz, the measured current will show an increase under fault condition which can be used as a measure to detect turn fault. A PM motor is usually fed from a pulse width modulated (PWM) drive which generates not only the fundamental voltage for the motor, but also HF voltage ripples at the terminals due to its switching. Therefore a PWM drive by nature of its operation generates HF voltage in the frequency range of interest, and the resultant HF PWM current ripple can be used as detector for inter-turn faults. For

the purpose of simulation in this paper a sine-PWM drive, with a switching frequency of 10 kHz is assumed.

In order to have the winding circuit model more realistic to the actual physical measurements, a hybrid modelling approach is employed. This entails using the impedance/admittance data obtained from experiments and combining it with the analytical model to obtain a closer representation of the actual circuit condition. First the data obtained from experiment is fitted with a transfer function (2) using least squares fitting to obtain $Y_{f,expt}(s)$. Fig. 4 shows the fitting for 20 turn fault case. Data from healthy ($Y_{h,expt}(s)$) and 2 turn fault can be fitted similarly.

$$Y(s) = \frac{b_4 s^4 + b_3 s^3 + b_2 s^2 + b_1 s^1 + b_0}{a_5 s^5 + a_4 s^4 + a_3 s^3 + a_2 s^2 + a_1 s^1 + a_0} \quad (2)$$

In order to use the fitted transfer function for simulation the faulted winding equations are analysed. Fig. 5 shows the schematic of winding with fault in phase 1 (faulted phase) connected to a five phase inverter. Since the winding admittance is a high order function, the model equations needs to be properly calculated to enable numerical simulation. The circuit equations of the faulted winding in s domain are given by (3)-(4). I_2 can be eliminated from the voltage equation (3) to obtain (5)-(6).

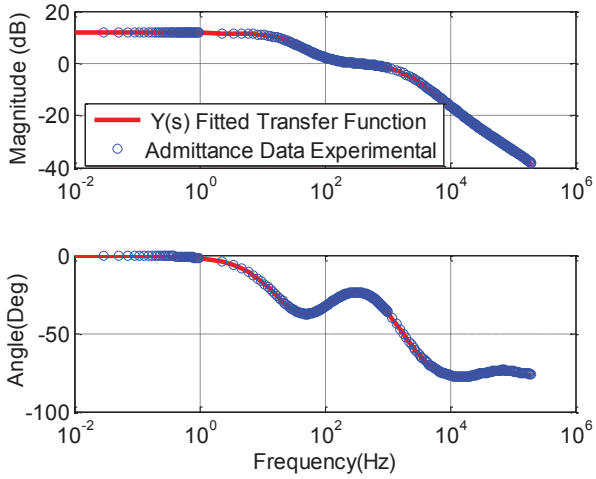

Fig. 4: Fitted Admittance Function

$$0 = R_2 I_2(s) + sL_s I_2(s) + sM I_1(s) + E_2(s) \quad (3)$$

$$V_1(s) = R_1 I_1(s) + sL_h I_1(s) + sM I_2(s) + E_1(s) \quad (4)$$

$$V_1(s) = \left(R_1 + sL_h - \frac{s^2M^2}{sL_s + R_2}\right) I_1(s) - \frac{sM}{sL_s + R_2} E_2(s) + E_1(s) \quad (5)$$

$$V_1(s) = \frac{1}{Y_f(s)} I_1(s) - \frac{sM}{sL_s + R_2} E_2(s) + E_1(s) \quad (6)$$

A closer look at (6) reveals that the first term corresponds both to the high frequency and low frequency admittance, whereas the other two terms are only related to the back-emf components. Hence, it is possible to substitute the experimentally derived admittance instead of the theoretically derived one, resulting in the hybrid model equation for the faulted phase in (7). Therefore, (7) contains a part of parameters obtained through experiment and the rest is calculated from theoretical model, and is called a hybrid model.

$$V_1(s) = \frac{1}{Y_{f,expt}(s)} I_1(s) - \frac{sM}{sL_s + R_2} E_2(s) + E_1(s) \quad (7)$$

Since the voltages generated by the inverter are w.r.t the negative DC supply N and the neutral 'n' of the motor is floating, the zero sequence voltage needs to be accounted for in the model as shown in (8). The model for other healthy windings can be derived by setting the admittance function to $Y_{h,expt}(s)$ (9). V_{nN} can be calculated by summing (8)-(9) over all phases, and noting that the sum of currents is zero, to obtain (10).

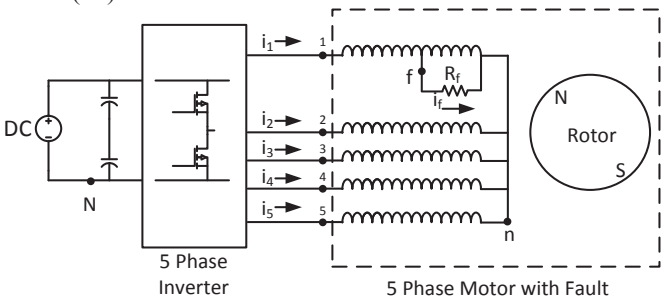

Fig. 5: Schematic representation of 5 phase SPM machine with turn fault on a single phase.

$$V_{1N}(s) = \frac{1}{Y_{f,expt}(s)} I_1(s) - \frac{sM}{sL_s + R_2} E_{fn}(s) + E_1(s) - E_{fn}(s) + V_{nN} \quad (8)$$

$$V_{iN}(s) = \frac{1}{Y_{h,exptt}(s)} I_i(s) + E_i(s) + V_{nN}\ ;\ \forall\, i \neq 1 \quad (9)$$

$$\sum V_{iN}(s) = \frac{1}{Y_{f,expt}(s)} I_1(s) - \frac{1}{Y_{h,expt}(s)} I_1(s) - \frac{sM}{sL_s + R_2} E_{fn}(s) - E_{1f}(s) + 5V_{nN} \quad (10)$$

The final model equation can then be derived by subtracting (10) from (8)-(9) to obtain (11)-(12) which forms the final set of model equations used in simulation study of the inter-turn fault signature under PWM operations.

$$V_{1N}(s) - \frac{\sum V_{iN}(s)}{5} = \left(\frac{4}{5}\frac{1}{Y_{f,expt}(s)} + \frac{1}{5}\frac{1}{Y_{h,expt}(s)}\right) I_1(s) + - \frac{4}{5}\frac{sM}{sL_s + R_2} E_{fn}(s) + E_1(s) - \frac{4}{5} E_{fn}(s) \quad (11)$$

$$V_{iN}(s) - \frac{\sum V_{iN}(s)}{5} = \frac{1}{Y_{h,expt}(s)} I_i(s) - \frac{1}{5}\left(\frac{1}{Y_{f,expt}(s)} - \frac{1}{Y_{h,expt}(s)}\right) I_1(s) + \frac{1}{5}\left(\frac{sM}{sL_s + R_2} + 1\right) E_{fn}(s), \qquad \forall\, i \neq 1 \tag{12}$$

3 Detector Design

In order to extract the high frequency current, first an appropriate frequency band needs to be selected. In order to quickly perform the design process, the harmonic currents needs to be calculated quickly under different operating conditions in steady state. The PWM harmonic voltages can be calculated using (13), where M_i is the ith phase modulation index defined as $M_i = V_i/(V_{dc}/2)$, ω_c , ω_f is the angular frequency of the carrier and fundamental waveform respectively and J_o and J_n denote the Bessel functions of orders 0 and n, respectively [13]. Harmonic line currents can be calculated using (14), where $Z_f(j\omega) = 1/Y_{f,expt}$ and $Z_h(j\omega_f) = 1/Y_{h,expt}$ represents the impedance of the faulted phase and healthy phase respectively.

$$V_{i,h}(t) = + \frac{2V_{dc}}{\pi} \sum_{m=1}^{\infty} \frac{1}{m} J_0\left(m\frac{\pi}{2}M_i\right) \cos(m\omega_c t) \sin\left(m\frac{\pi}{2}\right) + \frac{2V_{dc}}{\pi} \sum_{m=1}^{\infty} \sum_{n=1}^{\infty} \frac{1}{m} J_n\left(m\frac{\pi}{2}M_i\right) \cos\left(m[\omega_c t] + n[\omega_f t + \theta_i]\right) \sin\left([m+n]\frac{\pi}{2}\right) \tag{13}$$

$$\begin{bmatrix} V_{1,h} - V_{2,h} \\ V_{2,h} - V_{3,h} \\ V_{3,h} - V_{4,h} \\ V_{4,h} - V_{5,h} \end{bmatrix} = \begin{bmatrix} Z_f & -Z_h & 0 & 0 \\ 0 & Z_h & -Z_h & 0 \\ 0 & 0 & Z_h & -Z_h \\ Z_h & Z_h & Z_h & 2Z_h \end{bmatrix} \begin{bmatrix} I_{1,h} \\ I_{2,h} \\ I_{3,h} \\ I_{4,h} \end{bmatrix} \tag{14}$$

Fig. 6(a) shows the rms harmonic current plots for each phase when phase 1 has a 2-turn fault at the maximum current of 6A when only 10 kHz carrier frequency sidebands are considered and Fig. 6(b) shows the rms harmonic current plots when both 10 kHz and 20 kHz carrier frequency sidebands are considered. As is evident in the plots considering both the 10 kHz and 20 kHz current ripple a greater separation between the faulted phase and healthy phases can be obtained. Thus, a pass-band of 10-20 kHz is selected for optimal detection of fault. The separation in rms current ripples between faulted and healthy phases allow for ease identification of fault. It should be noted that the harmonic voltages and hence the harmonic currents are a function of modulation index and therefore as speed or load change the harmonic currents also vary but the difference between the healthy and faulted phases provides the means of the fault detection.

In order to extract the harmonic currents a signal processing chain, as shown in Fig. 7, consisting of a second order band-pass filter, RMS detector and output buffer, is employed. The band-pass (BP) filter must provide sufficient attenuation at fundamental frequency to prevent changes in fundamental current from affecting the result of the RMS detector. For the particular motor, a stop-band attenuation of -38dB is found to be adequate to remove the fundamental current influence. The pass-band gain of 20 dB is found to be sufficient for the detection. The bode gain plot of the BP filter is given in Fig. 8. The output buffer provides a further gain of +26dB.

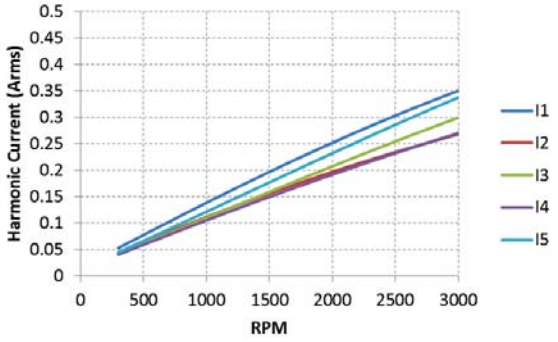

Fig. 6(a): RMS harmonic current (10kHz carrier and sidebands only)

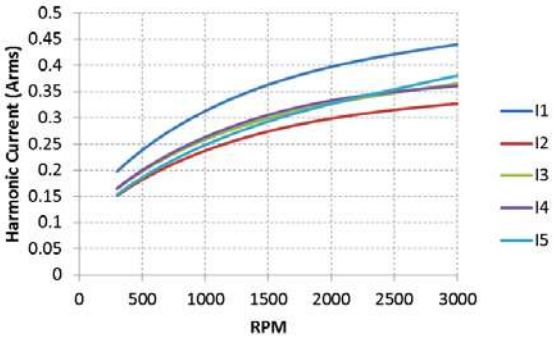

Fig. 6(a): RMS harmonic current (10kHz and 20kHz carrier frequency harmonics and sidebands)

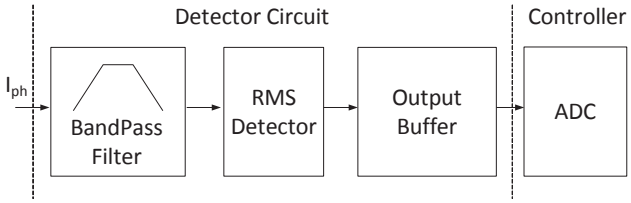

Fig. 7: HF detection Signal Chain

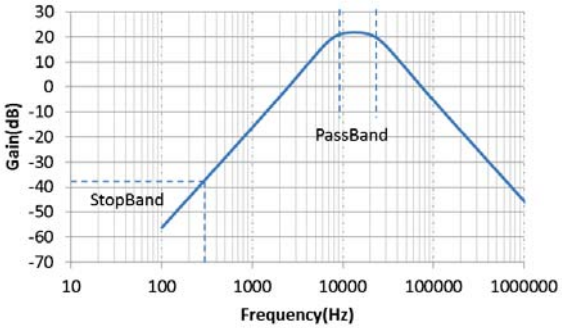

Fig. 8: Band-pass Filter Bode Plot

4 Circuit Implementation

Fig. 9 shows the schematic of the analog signal processing circuit. The current signal from the transducer is first fed to the high pass filter (HPF) and then through the low pass filter (LPF) into the RMS detector and finally into the ADC pre-amplifier (preamp). Since the LEM current sensor selected for the inverter is LTS-25P which gives a unipolar output, the entire HF signal chain is designed to operate on unipolar supply. To realise the LPF and HPF transfer functions multiple-feedback topology is used since it is easier to use the circuit in unipolar application. OPA364 is selected as the operational amplifier (opamp) for the circuit due to its excellent BW and low offset voltage and is suitable for unipolar circuit realisation. The RMS detector is LTC1968 which is a precision wide bandwidth, RMS-to-DC converter from Linear Technology [14]. LTC1968 has a differential input range of $1V_{pk}$ and to avoid saturating the RMS detector under worse case fault, a gain of 10dB is selected for the HPF and LPF in their pass-band. Finally the ADC preamp provides additional gain on the detected RMS value. A point to be noted for the signal chain is that the sequence of the block in the chain is critical to obtaining the desired performance. For example, swapping the position of HPF and LPF in the signal chain would saturate the opamps in the circuit although the transfer function of the circuit would have remained unaltered. This is because the LPF will pass the fundamental current signal with a gain of +10dB and will saturate the opamps in the circuit.

5 Results

Fig. 10-11 shows the simulation results from transient motor and detector model obtained at 500 RPM with iq = 6A under a 2 turn fault condition. The switching frequency of the inverter is set at 10 kHz. Note that the difference in high frequency ripple is hardly discernible in the actual phase current plots, however is clearly identifiable in the filtered RMS current plot, where phase-1 shows a higher ripple current and hence is identified as the phase with fault. The ripple in the filtered RMS current is caused by the currents in sidebands of the carrier frequency which give rise to a beat frequency at twice the fundamental frequency.

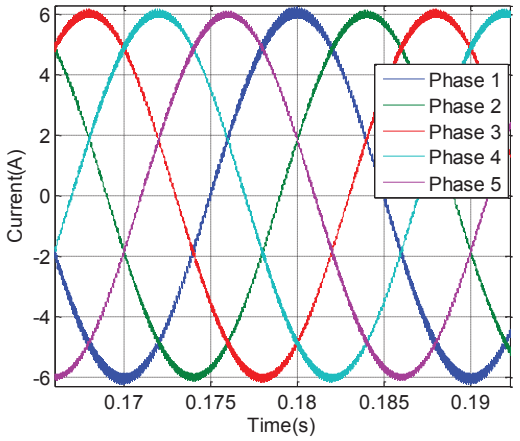

Fig. 10: Phase Currents @ 500 RPM
(Phase 1 has 2 turn fault)

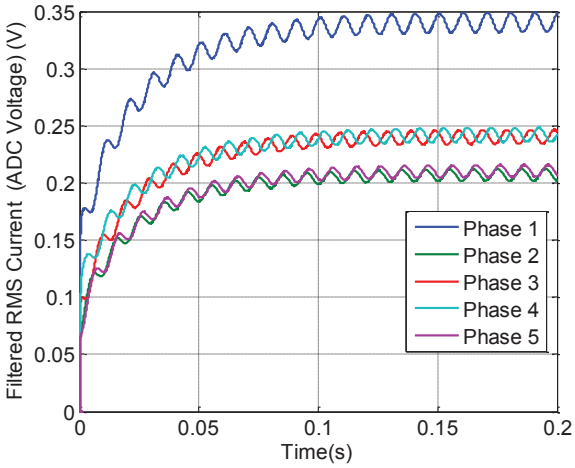

Fig. 11: Filtered HF RMS currents (V_{ADC}) @ 500 RPM
(Phase 1 has 2 turn fault)

Fig. 12-13 shows the transient model results obtained at 2000 RPM with iq = 6A and shows similar result as compared to the 500RPM case, although with higher harmonic current magnitude. This is expected since the harmonic currents are a function of modulation index and as the speed and load changes the harmonic currents also changes with it.
Detection of turn fault can be simply based on detection of

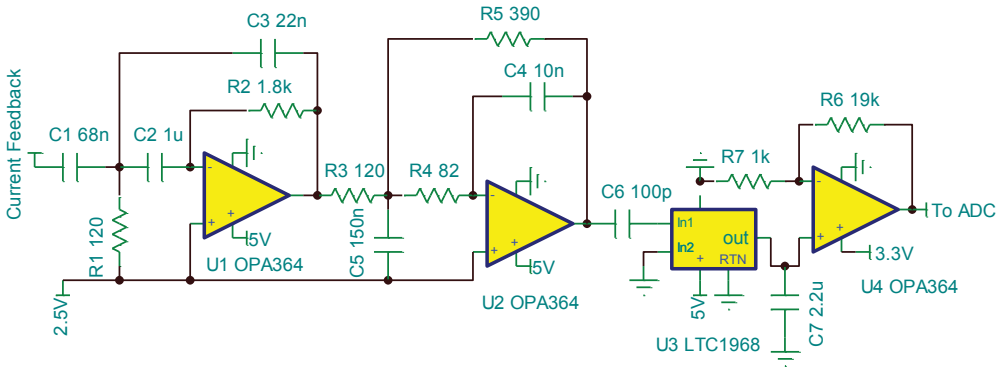

Fig. 9: Detector Circuit

difference of HF currents between phases. Under healthy condition the HF currents are expected to be close to each other, since the motor is more or less electrically balanced but under fault condition the difference in the RMS ripple currents will increase and can be used as method of fault detection. An alternative is to implement a variable fault threshold algorithm which changes the fault threshold limit with loading and speed, and can be easily implemented in DSP.

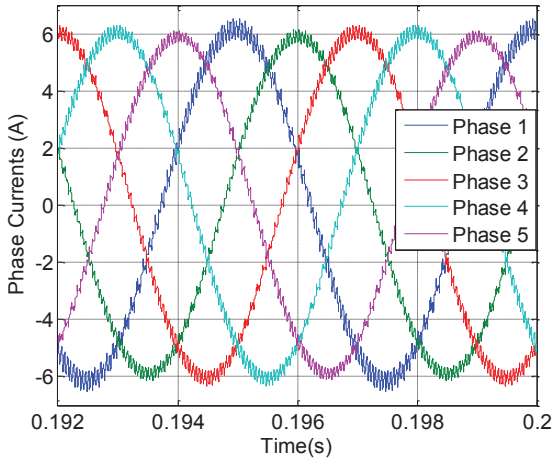

Fig. 12: Phase Currents @ 2000 RPM (Phase 1 has 2 turn fault)

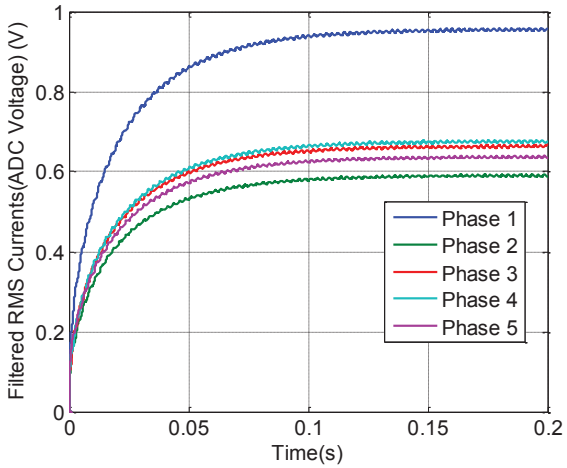

Fig. 13: Phase Currents @ 2000 RPM (Phase 1 has 2 turn fault)

Conclusion

A new method to detect turn fault using PWM ripple currents has been proposed in the paper. A machine model using measured high frequency winding parameters to accurately capture the high frequency behaviour of the winding is developed. Based on the analytical simulations a detector circuit to extract the PWM ripple current is designed. Transient simulation of the motor model with the detector model is shown to have good turn fault detection capability.

Acknowledgements

The authors gratefully acknowledge the European Commission, ENIAC JU and MotorBrain project partners for permission of the publication of this paper.

References

[1] Z. Q. Zhu and D. Howe, "Electrical Machines and Drives for Electric, Hybrid, and Fuel Cell Vehicles," *Proc. IEEE*, vol. 95, no. 4, pp. 746 – 765, Apr. 2007.

[2] A. H. Bonnett and C. Yung, "Increased Efficiency Versus Increased Reliability," *IEEE Ind. Appl. Mag.*, vol. 14, no. 1, pp. 29–36, 2008.

[3] "Report of Large Motor Reliability Survey of Industrial and Commercial Installations, Part I," *IEEE Trans. Ind. Appl.*, vol. IA-21, no. 4, pp. 853–864, 1985.

[4] "Report of Large Motor Reliability Survey of Industrial and Commercial Installations, Part II," *IEEE Trans. Ind. Appl.*, vol. IA-21, no. 4, pp. 865–872, 1985.

[5] A. H. Bonnett and G. C. Soukup, "Cause and analysis of stator and rotor failures in three-phase squirrel-cage induction motors," *IEEE Trans. Ind. Appl.*, vol. 28, no. 4, pp. 921–937, 1992.

[6] Y. Lee and T. G. Habetler, "An On-Line Stator Turn Fault Detection Method for Interior PM Synchronous Motor Drives," in *APEC 2007 - Twenty Second Annual IEEE Applied Power Electronics Conference*, 2007, pp. 825–831.

[7] C. Bianchini, E. Fornasiero, T. N. Matzen, N. Bianchi, and A. Bellini, "Fault detection of a five-phase Permanent-Magnet machine," in *34th Annual Conference of IEEE Industrial Electronics, 2008. IECON 2008*, 2008, pp. 1200–1205.

[8] J. Quiroga, L. Liu, and D. A. Cartes, "Fuzzy logic based fault detection of PMSM stator winding short under load fluctuation using negative sequence analysis," in *American Control Conference, 2008*, 2008, pp. 4262 –4267.

[9] F. Briz, M. W. Degner, A. Zamarron, and J. M. Guerrero, "Online stator winding fault diagnosis in inverter-fed AC machines using high-frequency signal injection," *IEEE Trans. Ind. Appl.*, vol. 39, no. 4, pp. 1109–1117, 2003.

[10] J. Arellano-Padilla, M. Sumner, and C. Gerada, "Winding condition monitoring schemefor a permanent magnet machine using high-frequency injection," *IET Electr. Power Appl.*, vol. 5, no. 1, pp. 89–99, 2011.

[11] B.-M. Ebrahimi and J. Faiz, "Feature Extraction for Short-Circuit Fault Detection in Permanent-Magnet Synchronous Motors Using Stator-Current Monitoring," *IEEE Trans. Power Electron.*, vol. 25, no. 10, pp. 2673–2682, 2010.

[12] Z. Sun, J. Wang, D. Howe, and G. Jewell, "Analytical Prediction of the Short-Circuit Current in Fault-Tolerant Permanent-Magnet Machines," *IEEE Trans. Ind. Electron.*, vol. 55, no. 12, pp. 4210 –4217, Dec. 2008.

[13] D. G. Holmes and T. A. Lipo, 'Pulse Width Modulation for Power Converters: Principles and Practice', Wiley-IEEE Press, 2003.

[13] "LTC1968- RMS-to-DC Converter - Linear Technology." [Online]. Available: http://www.linear.com/product/LTC1968. [Accessed: 09-Jan-2014].